Accepted Article

Title: The deposition of the spin crossover Fe(II)-pyrazolylborate complex on Au(111) surface at molecular level

Authors: Nicolás Montenegro-Pohlhammer, Rocío Sánchez-de-Armas, and Carmen J. Calzado

WILEY-VCH

The deposition of the spin crossover Fe(II)-pyrazolylborate complex on Au(111) surface at molecular level

Nicolás Montenegro-Pohlhammer,[a] Rocío Sánchez-de-Armas[a] and Carmen J. Calzado[a]*

[a]Departamento de Química Física. Universidad de Sevilla. c/ Profesor García González, s/n. 41012 Sevilla. Spain.

*Corresponding author: calzado@us.es

ABSTRACT

The interaction at molecular level of the spin-crossover $Fe^{II}((3,5-(CH_3)_2Pz)_3BH)_2$ complex with the Au(111) surface is analyzed by means of rPBE periodic calculations. Our results show that the adsorption on the metallic surface enhances the transition energy, increasing the relative stability of the low spin (LS) state. The interaction indeed is spin-dependent, stronger for the low spin than the high spin (HS) state. The different strength of the Fe ligand field at low and high temperature manifests on the nature, spatial extension and relative energy of the states close to the Fermi level, with a larger metal-ligand hybridization in the LS state. This feature is of relevance for the differential adsorption of the LS and HS molecules, the spin-dependent conductance, and for the differences found in the corresponding STM images, correctly reproduced from the density of states provided by the rPBE calculations. It is expected that this spin dependence will be a general feature of the SCO molecule-substrate interaction, since it is rooted in the different ligand field of Fe site at low and high temperatures, a common hallmark of the Fe(II) SCO complexes.

Finally, the states involved in the LIESST phenomenon has been identify through NEVPT2 calculations on a model reaction path. A tentative pathway for the photoinduced LS$\rightarrow$ HS transition is proposed, that does not involve the intermediate triplet states, and nicely reproduces both the blue laser wavelength required for the activation, and the wavelength of the reverse HS $\rightarrow$LS transition.

1

INTRODUCTION

Spin-crossover (SCO) molecules can switch between two spin states under the influence of external stimuli such as temperature, pressure, light, magnetic and electric fields. [1],[2],[3],[4] The potential applications of the SCO molecules as displays, sensors and memories require the persistence of their spin-crossover properties once deposited on a substrate.[4],[5],[6],[7] Both the interaction with the substrate and the size reduction (to nanoparticles, ultrathin layers and down to the molecular scale) can induce strong modifications of the SCO properties, such as the change in transition temperature,[7],[8] the coexistence of the two spin states at low temperature[9],[10],[11],[12],[13] or even the complete suppression of the spin transition.[14]

Additionally, to prepare high purity objects on the surface is also a challenge.[1, 15] There are many Fe^{II} and Fe^{III} complexes exhibiting SCO properties, but only a reduced number of them are well suited for sublimation techniques under high-vacuum conditions.[12],[15],[16],[17],[18],[19] One of them corresponds to the $Fe^{II}((3,5-(CH_3)_2Pz)_3BH)_2$ (Fe-pz) complex, Pz= pyrazolyl. This Fe-pz complex exhibits a transition between a S=0 low-spin (LS) state and a S=2 high-spin (HS) state. [18, 20] In the form of a powder, the molecule presents an asymmetric hysteresis, with transition temperatures of $T_{HS \rightarrow LS}$ =174K and $T_{LS \rightarrow HS}$=199K,[17] 205K.[18, 21] When thick Fe-pz films were deposited on Si(100)/SiO$_2$ and quartz substrates by thermal evaporation,[17] the SCO properties were preserved, but the transition temperatures shifted towards lower temperatures when the film thickness decreased.[17] These size-dependent SCO characteristics have been previously reported for nanocrystals and thick films of other Fe(II) SCO complexes, such as [Fe(H$_2$B(pz)$_2$)$_2$(bipy)] and [Fe(H$_2$B(pz)$_2$)$_2$(phen)] deposited on different substrates.[16] Additionally to the size effects, the Fe-pz thin-film on Si/SiO$_2$ and quartz substrates retained a non-negligible fraction of the HS state at low temperature, i.e., the spin-state switching is not complete at low temperature. Optical and magnetic measurements on Fe-pz films with thicknesses ranging from 90 to 8460 nm showed that the fraction of HS molecules at low temperature is due to a metastable phase triggered by the sublimation, which can be transformed into the stable one by annealing.[18]

Going down to thicker films, recently Bairagi et al.[11] characterized a single layer of Fe-pz in direct contact with Au(111). At 4.6 K a long-range superstructure was formed with one molecule in HS state and two molecules in the LS state. The illumination with blue light induced the LS to HS switching and the formation of a photoinduced superstructure with one molecule in HS state and one molecule in LS state.[21] Then the SCO can be induced by light for molecules in direct contact with the metallic substrate. This mixed phase of HS and LS states at low temperature, evidenced by the STM, were confirmed by a posterior XAS study,[21-22] and also demonstrated the thermal and soft X-ray-induced spin crossover of the Fe-pz layer deposited on Au(111) substrate. The structure of the Fe-pz submonolayer in contact with Au(111) was recently determined by means of grazing incidence X-ray diffraction (GIXD) measurements, combined with DFT+U calculations.[23] The molecular layer exhibits an epitaxial relationship with the metallic substrate, and the resulting epitaxial strain have been suggested as responsible for the presence of the mixed spin state at low temperature, based on a simple mechanoelastic model. DFT+U calculations on a three-molecule unit cell confirmed that the mixed phases have significantly lower energies than the pure phases, but these calculations are strongly dependent on the U parameter, which represents the on-site Coulomb repulsion

of the Fe 3d electrons. In fact, the mixed spin state is more stable than the pure spin state only for a dramatically narrow window of U values, between U=6.5 and 6.6 eV.[24] The finally adopted value of U=6.55 eV is out of the range of values (2.5 to 5.6 eV) usually employed for DFT+U calculations on Fe SCO complexes.[24],[25],[26],[27],[28],[29],[30]

The aim of this work is to explore in depth the interaction of the Fe-pz complex with the Au(111) surface at a molecular scale, trying to shine light on the spin-state dependence of different features such as (i) the relative stability of the LS and HS states once deposited, (ii) the adsorption energies, (iii) the differential conductance of the HS and LS states and (iv) the origin of the LIESST phenomenon. The strong dependence found on U parameter on the reported LDA+U calculations[24] prompts us to look for alternative theoretical procedures to safely and unambiguously analyze the deposition of the Fe-pz complex on Au(111). We use state-of-the-art wavefunction-based approaches to establish the confidence range of some exchange-correlation functionals to be used in our periodic DFT calculations. We rest on non-hybrid functionals, computationally less demanding than the hybrid ones, and with contrasted good performance on the study of Fe(II) SCO complexes.[31],[32] Once the computational strategy is established, our results show for the first time that the Fe-pz complex exhibits a differential interaction with the Au(111) surface as a function of the spin state. The LS→ HS transition energy is modified by the presence of the substrate. The states involved in the LIESST phenomenon have been characterized, and a tentative pathway for the photoinduced LS→ HS transition has been suggested. Both the simulated STM images and I-V curves of the deposited complex are in excellent agreement with the experimental data and can be rationalized on the basis of the density of states close to the Fermi level.

The whole study is centered on an isolated molecule on the metallic surface. Our results indicate that the chosen computational strategy is robust enough to describe the deposition of the Fe-pz on the metallic substrate. The next step is to deal with a Fe-pz submonolayer representative of the $S_{1/3}$ superstructure observed by STM.[11, 24] This would be addressed in a forthcoming paper, where the role of the intermolecular interactions on the persistence of the HS state at low temperature will be analyzed.
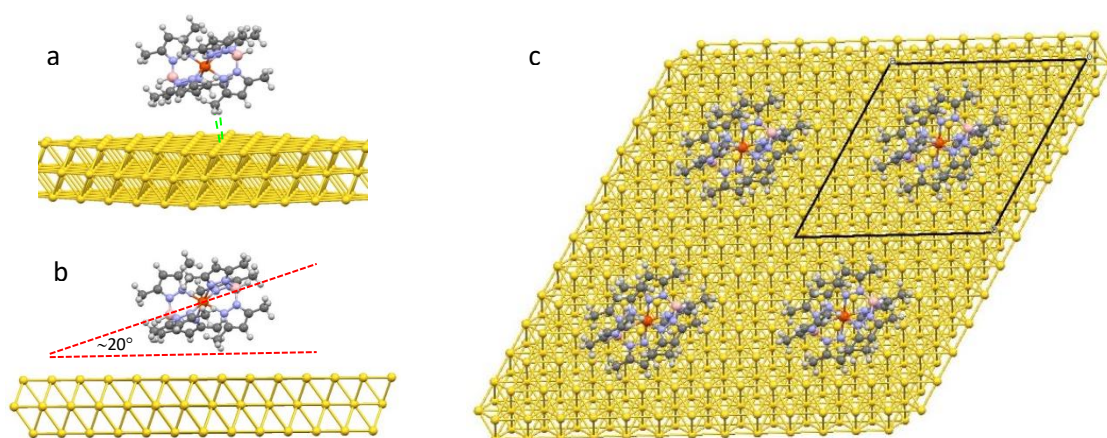

Figure 1. Fe-pz molecule on Au(111). a) The green lines represent the closest contacts between the molecule and the surface. b) The molecule is titled towards the surface, the B-Fe-B axis forms an angle

3

of ~20° with the surface. c) The unit cell employed in the periodic calculations (in black) is replicated along *a* and *b* directions, the intermolecular distance is large enough to prevent intermolecular interactions. Yellow, brown, pink, blue, gray and white represent, respectively, Au, Fe, B, N, C and H atoms.

COMPUTATIONAL DETAILS

Isolated molecule

The relative stability of the LS and HS states of the isolated molecule has been evaluated on the basis of the multiconfigurational second order theory (CASPT2[33] and NEVPT2[34] approaches). The reference wavefunction for each state is obtained from complete active space self-consistent field CASSCF calculations. The active space of the CASSCF wavefunctions contains ten electrons and twelve orbitals, as in previous studies on SCO complexes.[35],[36],[37],[38],[39],[40] The active orbitals include five 3d Fe orbitals, a second 3d shell to properly account for dynamical correlation effects of the 3d electrons, and two eg-like occupied N ligand orbitals, that introduce the effect of the ligand-to-metal charge transfer (LMCT) due to the σ-donation of the N ligands. To avoid the presence of intruder states and to provide a balanced description of open and closed shells CASPT2 calculations were performed using an imaginary level shift of 0.20 a.u. and IPEA shifts ranging from the default value of 0.25 a.u. to 0.5 a.u.[41] In fact, there is not a common agreement about the use of the default IPEA value when dealing with problems such as the evaluation of the magnetic coupling constants and the relative stability of the HS and LS states of SCO molecules. Values ranging from 0.25-0.7 au can be found in literature for studies focusing on SCO molecules (for instance, Refs. 35-40). Due to this long-running controversy,[42] a set of IPEA values have been explored to establish the upper and lower limits of the HS-LS energy within this approach.

Scalar relativistic effects were included using a Douglas-Kroll Hamiltonian.[43] All CASSCF/CASPT2 calculations were performed using the Molcas 8.0 package,[44] with ANO-RCC basis sets[45] with contraction [5s4p3d2f1g] for Fe, [4s3p1d] for N, [3s3p1d] for C and B, and [2s] for H.

Additionally, the energy of the LS and HS states were also evaluated on the basis of the N-Electron Valence State Perturbation Theory (NEVPT2) developed by Angeli *et al.*[34, 46] using the ORCA implementation.[47] With respect to CASPT2 this approach has the advantage of being parameter free and avoiding the intruder state problem. State specific CASSCF wavefunctions were employed as zeroth-order wavefunctions. All CASSCF/NEVPT2 calculations were performed using the def2-TZVP basis set[48] for all atoms, except the Fe ion, where a def2-QZVP basis was employed.[48] Relativistic effects are introduced through the zeroth-order regular approximation (ZORA).[49] In order to achieve the required precision in the energy values, all electrons in the molecule were considered in the SCF process, and the parameters D3Tpre and D4Tpre were set to 0.

The ligand field strength of Fe center for the LS and HS states has been determined from the ab initio ligand field theory (AILFT) approach[50] implemented in ORCA. State-average CASSCF(6,5) calculations, with 6 electrons occupying the five 3d Fe orbitals, were carried out

4

for each spin multiplicity, with equal weights for all roots of each multiplicity (5 quintets, 45 triplets and 50 singlets).

Finally, to compare with the periodic results, the energy difference between the HS and LS states of the isolated molecule has been evaluated from density functional theory (DFT) based calculations with the revised Perdew-Burke-Ernzerhof functional (rPBE).[51] This functional has been proven to provide a good LS-HS balance for well-known SCO complexes containing Fe(II) and Fe(III).[31],[32] The effect of the van der Waals interactions were included through the D3 Grimme approach.[52]

Adsorption on Au(111)

The adsorption of a single molecule on Au(111) has been studied within periodic DFT calculations using the VASP (Vienna ab initio simulation package) code[53] employing the generalized gradient approximation (GGA) with the rPBE functional[51] and projector-augmented wave (PAW) potentials.[54] Valence electrons are described using a plane-wave basis set with a cutoff of 500 eV and the Γ-point of the Brillouin zone is used.[55] The optimized lattice parameters for the Au bulk are $a=b=c=2.97$ Å. This calculated value has been used for the (111) surface throughout the present work and maintained fixed during the atomic positions relaxation.

The Au(111) surface is represented by a slab containing 108 atoms and 3 layers (17.820 x 17.820 Å). The atoms of the two lowest layers are kept fixed at bulk optimized positions. 26 Å of vacuum have been added in the z direction to avoid the interaction between the slabs. Electronic relaxation has been performed until the change in the total energy between two consecutive steps is smaller than 10^{-6} eV and the ionic relaxation has been performed until the Hellmann-Feynman forces were lower than 0.025 eV/Å. As we are interested in the different magnetic solutions, the NUPDOWN option is used, which forces the difference between number of electrons in up and down spin channels, $N_\alpha-N_\beta$, to be equal to 0 (LS) or 4 (HS). Starting geometries for geometry optimizations have been selected from previous experimental and theoretical published data.[11, 23] These previous works state that the molecules are adsorbed on the Au(111) surface as a monolayer which unit cell parameters are close to those of the $(01\bar{1})$ crystallographic plane of the bulk structure at 298 K.

The adsorption energies, E_{ads}, were calculated with respect to an isolated molecule on a 17.820×17.820×32 Å^3 box as $E_{ads}=E_{adsorbed\_molecule} - (E_{slab}+E_{molecule})$. Thus, negative adsorption energies represent bound states. The dimension of the unit cell assures that the deposited molecules do not interact with each other (Figure 1), the closest H….H contacts between –CH$_3$ groups of neighbor molecules along *a* and *b* axis are found at 6.9 Å and 8.1 Å, respectively. Then the calculated adsorption energies just correspond to the molecule-surface interaction.

In order to check the dependence of the technical parameters on the results, we have also done geometry optimizations employing PBE[56] and rev-PBE[57] GGA functionals and the meta-GGA functional SCAN[58] as well as including Van der Waals interactions through the DFT-D2[59] (PBE-D2) or the DFT-D3[52] method of Grimme (PBE-D3 and rPBE-D3).

The STM simulations with two different bias voltage (-1 and 1 V) were carried out using the Tersoff-Hamann approximation.[60] Constant-height STM images were finally visualized in the

5

p4vasp program using density values of 0.00 and 0.05 e/Å^3 as low and high boundaries, respectively. Finally, optical spectra were simulated using the imaginary part of the frequency-dependent dielectric function $\varepsilon_2(\omega)$, as proposed by Gajdoš et al.[61]

Transport properties

The spin-resolved transport properties of the complex, in both its high (HS) and low spin (LS) configurations, adsorbed on the gold surface, were studied through the DFT-Non equilibrium Green Functions Theory (NEGFT) methodology.[62] In order to recreate the experimental conditions as realistic as possible, we devised two molecular-junction configurations featuring the Fe complex in both configurations (HS and LS) as the active magnetic center, a slab of the Au(111) surface, extending perpendicular to the $(01\bar{1})$ plane as one of the electrodes, and a nano-wire of Au(111) exhibiting a pointed end at the molecule, as the other opposing lead (Figure 2). This setup was selected having in mind that it has been suggested that the STM tip probably aligns with the molecular z-axis, [11] who pass through both B atoms, and extends in this direction, through the surface $(01\bar{1})$ plane. Thus, this axis was selected as the device z-axis, and the direction from the surface to the tip, as the negative transport direction.

The electronic transport properties were performed by means of TRANSIESTA and TBTRANS modules[63] of SIESTA[64] package, based in a combination of DFT and the Keldysh nonequilibrium Green´s function (NEGF) formalism.[62] The mesh cut-off energy was set to 300 Rydberg for both the real and reciprocal space grids in all calculations, with a self-consistency tolerance for the convergence of the Hamiltonian and density matrices of 10^{-4} eV. All the atoms were represented by a double-zeta polarized (DZP) basis set, along with Troullier–Martins pseudopotentials,[65] employing the PBE exchange-correlation functional, due to convergence problems found when using the rPBE functional with TRANSIESTA code. Moreover, PBE is the functional most used for evaluating the transport properties on molecular junctions through the DFT-NEGFT methodology,[66],[67],[68] employed in several recent studies with Fe-SCO complexes as magnetic active elements.[69],[70],[71],[72],[73]
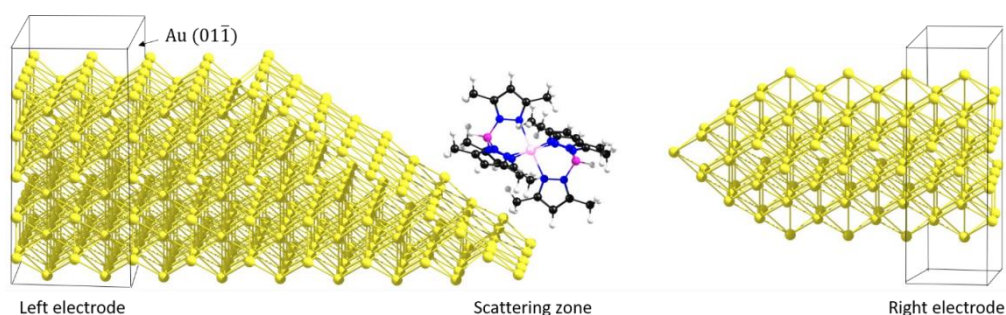

Figure 2. Molecular junction scheme employed in the transport properties calculations.

LIESST mechanisms

To get insight into the LIESST mechanism of the Fe-pz complex, the potential energy surfaces of all relevant low-lying spin states have been evaluated. A set of intermediate structures were

6

generated from the X-ray structure of the low and high temperature phases. The internal coordinated of the ligands were kept frozen to the low temperature X-ray structure (the LS state), while the distance between the Fe-N ligands were continuously varied from the LS structure to the high-temperature HS structure. The average Fe-N distance was chosen as reaction coordinate. It is worth noting that the CH_3 groups of the pz ligands present a slightly different orientation on the LS and HS structures. For this reason, the minimum in the quintet state curve appears slightly shifted to smaller average Fe-N distances than in the experimental high-temperature structure. This could affect the precise positions of the intersystem crossing points. But certainly it does not affect the vertical transitions from the ground singlet state curve, which determine the LIESST phenomena at low temperature, since the structure for the minimum of the ground singlet state corresponds exactly to the low-temperature x-ray structure.

The potential energy curves of the low-energy states of the Fe-pz complex as function of the Fe-N distances were evaluated using CASSCF/NEVPT2 calculations. The effects of spin−orbit coupling on the relative energies between the different electronic states are only minor and have not been included.[36, 39] The reference wavefunction for each point on the energy profile was obtained from the average of the first five roots of quintet, triplet and singlet states. A NEVPT2 calculation was performed on the top of each converged SA-CASSCF wavefunction, using the default parameters of ORCA code.

RESULTS

### Benchmark calculations: the isolated molecule

In a first step, we have evaluated the energy difference between the HS and LS states, referred as HS-LS. The purpose is to establish a confidence range for the DFT-based calculations, using as reference the results provided by wavefunction (WF) based methods.

The X-ray data for the low temperature and high-temperature phases are employed to determine the energy of the LS and HS states, respectively. The HS-LS energy is evaluated from CASSCF/CASPT2 and CASSCF/NEVPT2 calculations, and compared to the value resulting from a DFT evaluation with rPBE functional. Table 1 shows the almost linear dependence on the IPEA shift for the CASPT2 results, with HS-LS energies ranging from 12 to 28 kJ/mol for increasing IPEA values. The HS-LS values are in line with those obtained from NEVPT2 calculations, with the strongly contracted (20 kJ/mol) or the partially contracted (9.7 kJ/mol) schemes.[46] The estimates provided by the wavefunction-based approaches are in agreement with the experimental value for the transition enthalpy[18] of ΔH_{HL} =10.2 kJ/mol for the bulk structure. When comparing with the experimental data it should be noted that our evaluations do not take into account the intermolecular interactions present in the crystal. Then if they are relevant for the transition, i.e. one of the states is differentially stabilized by them,[28] this contribution to the transition energy would not count as part of our estimates.

7

Table 1. Energy difference between the HS and LS states (kJ/mol) for the isolated Fe-pz molecule, calculated on the basis of the low and high temperature X-ray bulk structures for the LS and HS states, respectively, or from the optimized geometries of each spin state using the rPBE functional. D3 refers to Grimme dispersion correction. ZPC is the zero-point correction.

Method & geometry employed			HS-LS / kJ mol^{-1}
CASPT2	X-ray data	IPEA= 0.25 au	12.1
		IPEA= 0.4 au	22.1
		IPEA= 0.5 au	28.3
NEVPT2	X-ray data	Partially contracted	9.7
		Strongly contracted	20.3
rPBE	X-ray data		54.1
rPBE	Optimization		10.0
rPBE + ZPC	Optimization		1.3
rPBE + D3	Optimization		52.7
rPBE + D3 + ZPC	Optimization		44.0
ΔH_{HL} exp			10.2

The ligand field strength of Fe site on each spin state has been evaluated by means of the ab initio ligand field theory (AILFT) approach implemented in ORCA. Scheme 1 reports the energy values of the ligand field one-electron functions resulting from the AILFT analysis. As expected, the gap is definitively larger for the LS state. The separation between the barycentres of the t2g and eg-like orbitals is of 16189 cm^{-1} for the LS molecule, versus a separation of 9523 cm^{-1} for the HS state. This result is in line with the composition of the Fe 3d t2g-like and eg-like active orbitals of the HS and LS states. The ligand contribution is larger for LS than HS orbitals, particularly for the unoccupied eg-like orbitals. Thus, the Löwdin orbital analysis of the CASSCF orbitals gives a 87.8% of 3d Fe character for the eg-like orbitals of the LS state, versus 98.2% in the case of the HS state.
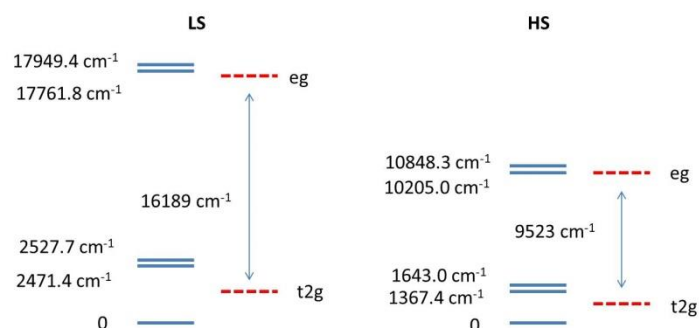
Scheme 1. Ligand field theory parameters for the LS and HS states of the isolated Fe-pz molecule.

8

When the HS-LS energy is evaluated from DFT calculations with the rPBE functional, the resulting energy difference is of 54 kJ/mol (Table 1), about five times larger than the experimental enthalpy. But, interestingly once the geometry of both states is optimized, the energy difference between them decreased to 10 kJ/mol, in excellent agreement with the experimental ΔH_{HL}. This result goes along with the general trend observed for this functional when dealing with SCO Fe complexes.[31-32] The optimized rPBE geometries of the isolated molecule compare well with the X-ray geometries of the crystal at low and high temperature, with a mean deviation of the Fe-N distances in the FeN_6 core of 0.05 Å and 0.08 Å for the LS and HS states, respectively. Part of this deviation can be related to the absence of packing effects in our calculations. Hence, it is extremely important for DFT-based approaches to ensure that the structures employed in the calculation correspond to minima in the corresponding potential energy surfaces, otherwise the HS-LS energy could be overestimated.

Comparing with previous DFT+U calculations, the rPBE functional presents two main advantages, it is a non-hybrid functional, relevant for the computational cost of the subsequent calculations of the molecule on the Au(111) surface, and it is parameter-free. In fact, LDA+U calculations of the Fe-pz complexes showed that the HS-LS energy difference is dramatically sensitive to the U value, much more than usual. In fact, it can be tuned from 2.5 eV (240 kJ/mol) to 0 eV by varying U from 0 to 6.88 eV. For $U \geq 6.9$, the HS state is favored over the LS state.[24]

Similar results are obtained from VASP calculations on the isolated molecule, using periodic conditions. The size of the unit cell (17.82Å x 17.82Å x 32Å; α 90°, β 90°, γ 60°) avoids any intermolecular interaction (Figure 1). Table 2 shows the HS-LS energy difference for different exchange-correlation functionals. PBE and SCAN largely overestimate the HS-LS energy, while the estimates obtained with the revised versions of PBE, rPBE and revPBE, are both in agreement with the values provided by the WF-based approaches. Nicely, the HS-LS energy difference for rPBE is in accordance with the value obtained from the calculation on the isolated molecule, without periodic conditions. Note that we compare two types of calculations: gas phase calculations of the isolated molecule at CASPT2, NEVPT2 and rPBE level using two different packages, MOLCAS and ORCA, and gas phase calculations with periodic conditions, at rPBE level, using VASP code. It is worth noting that each type of calculation introduces different approaches and makes use of different basis sets. For this reason, small deviations between the estimates resulting from these different treatments are expected.

When dispersion effects are included through Grimme corrections (D2[59] or D3[52] in Table 2), the low-spin state is largely favored, as previously noted,[32] resulting in highly overestimated HS-LS energies. The same is observed for finite calculations (rPBE+D3 entries in Table 1). Instead, zero-point corrections favored the HS state by 9 kJ/mol in average,[32] by 8 kJ/mol in our case (ZPC entries in Table 1). Since these two effects partially compensate and in particular, the zero-point corrections are difficult to be evaluated in a periodic frame, we decide to rest on the rPBE functional, without corrections, for subsequent studies using the periodic DFT approach.

9

Table 2. Periodic DFT evaluations of the HS-LS energy difference for the Fe-pz molecular crystal, the isolated molecule and the molecule/Au(111) with unit cell (17.82Å x 17.82Å x 32Å; α 90°, β 90°, γ 60).

System	Geometry	XC Functional	HS-LS (kJ/mol)
Molecular crystal	X-ray data	rPBE	29.5
Isolated molecule in periodic cell	Optimization	PBE	76.3
		rPBE	18.2
		revPBE	29.7
		SCAN	74.8
		PBE+D2	118.4
		PBE+D3	95.1
		rPBE+D3	65.5
Molecule on surface	Optimization	rPBE	25.1

Adsorption on Au(111) surface

In the following, we focus on the adsorption of the Fe-pz complex on the Au(111) surface and the impact on the spin transition. The molecule on the surface has been optimized in the LS and HS states, using as starting point the optimized geometries at DFT+U level reported by Fourmental et al.[23] In this structure, molecules are adsorbed on the Au(111) surface as a monolayer which unit cell parameters are close to those of the crystallographic plane $(01\bar{1})$ of the bulk structure at 298 K. In this orientation, the molecule is titled towards the surface, the B-Fe-B axis forms an angle of ~20° with the surface (Figure 1). In our case, the unit cell contains just one of these molecules. The *a* and *b* axes of the unit cell are large enough to avoid any intermolecular interaction.

The adsorption energies are spin-dependent, with values of −32.2 kJ/mol (−0.33 eV) for LS state and −25.3 kJ/mol (−0.26 eV) for the HS state. Then once deposited, the interaction with the substrate is weakened when temperature rises. These adsorption energy values are in better agreement with the expected weak molecule-substrate interaction,[11],[24] that the previous evaluations based on DFT+U calculations, which provide adsorption energies of ~2.1 eV (203 kJ/mol),[11] hardly classifiable as a weak interaction. The dependence of the adsorption energy with the spin state has been previously observed for the deposition of Fe(phen)$_2$(NCS)$_2$ on metallic substrates[30, 74] (−2.62 eV for LS and −2.22 eV for HS on Cu(100) surface). In such a case, the sulfur atoms of NCS ligands strongly bind the surface, and this would explain the coexistence of two spin states and the inability to switch found for Fe(phen)$_2$(NCS)$_2$ on Cu(100). Note that the calculated adsorption energies for Fe-pz are one order of magnitude smaller than that reported for Fe(phen)$_2$(NCS)$_2$. This is in line with the fact that SCO properties of Fe-pz are preserved once deposited, while the switching is blocked in the case of Fe(phen)$_2$(NCS)$_2$. Then it seems to exist a clear correlation between the strength of the interaction with the surface and the prevalence of the bistability.

10

The closest contact between the adsorbed molecule and the Au(111) surface takes place through two of the hydrogen atoms of one of the methyl groups (Figure 1). They occupied on-top positions at distances of 3.04 Å and 3.21 Å for the LS state, and 3.05 Å and 3.15 Å for the HS state. During the optimization the molecule maintains the same orientation in relation to the surface than in the optimized geometry obtained from DFT+U calculations, [24] but in the rPBE optimized system the molecules are considerably further to the surface (closest distances Au-H in the starting geometry were 2.42 Å and 2.51 Å for the LS state, and 2.49 Å and 2.39 Å for the HS state). Our results are consistent with lower adsorption energy values that reported before.

The deposition of the molecule on the metallic surface modifies the transition energy, which increases from 18.2 kJ/mol to 25.1 kJ/mol. Such an increase of the relative stability of the LS state due to the surface together with the larger adsorption energy of the LS molecules should increase the transition temperature of the deposited molecules, and should not favor the presence of a mixed HS and LS phase at low temperature observed for the monolayer of Fe-pz on Au(111) surface.[24] Then the origin of such a mixed phase is not in the interaction of each individual molecules with the substrate, but must be related to the intermolecular interactions and the structural constrains imposed to the molecular layer by the Au(111) surface, as suggest the toy mechanoelastic model of Fourmental *et al*.[24] These effects could modify not only the relative energies of the two spin states, but also the energy barrier between them. Works on these issues are in progress.
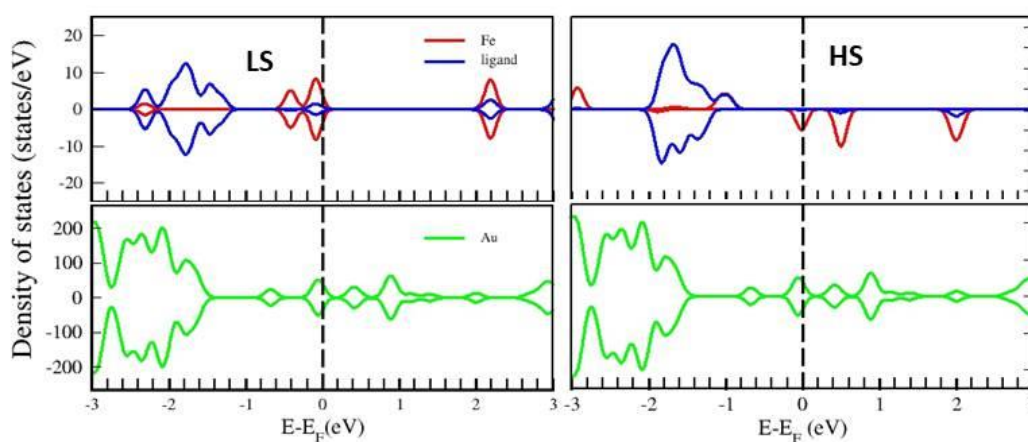

Figure 3. Projected density of states of the LS (left) and HS(right) molecule on Au(111) surface. Red, blue and green lines correspond to Fe, ligands and Au, respectively.

Figure 3 represents the Fe-, ligands- and Au-projected density of states of the molecule deposited on Au(111) for both spin states. The bands close to the Fermi level are mainly Fe 3d with a larger hybridization with the ligands for the LS state than for the HS one. This result is in line with the strength of the ligand field around the Fe site, larger for the low temperature geometry (the LS state), where the Fe-N distances are shorter than for the high-temperature geometry (the HS state). The shorter the Fe-N distances, the stronger the mixing of the ligand-centered orbitals with the Fe 3d ones. In consequence, the active orbitals of the LS state are

11

spatially more extended than the HS ones, as shown in Figure 4. This leads to frontier bands (orbitals) with a larger weight on the ligands for the LS molecules than for the HS ones (Figure 4). This result could be also related with the greater adsorption energy of the LS phases, since spatially more extended orbitals can promote stronger interactions with the surface. Hence, it is expected that this trend will be a general feature of the SCO molecule-substrate interaction, since it is rooted in the different ligand field of Fe site at low and high temperatures, a common hallmark of the Fe(II) SCO complexes.
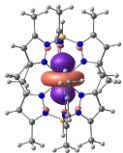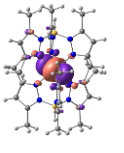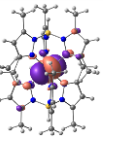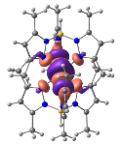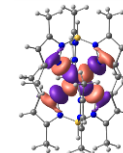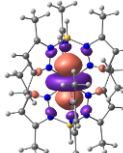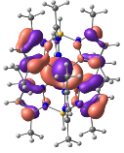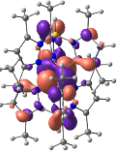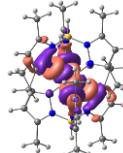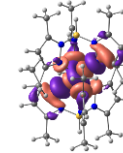
	t_{2g}-like			e_g-like	
HS					
occ	2	1	1	1	1
LS					
occ	2	2	2	0	0

Figure 4. Representation of the Fe 3d t_{2g}-like and e_g-like active orbitals for the HS (top) and LS (bottom) states obtained from rPBE calculations on the isolated molecule. occ refers to the occupation number of each orbital.

These frontier orbitals (bands) are responsible for the differences found in the STM images obtained with positive and negative bias voltage.[11] Experimentally, in positive bias, V, the electrons flow from the tip to the empty orbitals (states) of the sample placed between the Fermi level, E_F, and E_F+V eV. Since the tip is placed on the top of the molecule, the local states accessible for the tip electrons are those centered on the molecule. For the LS molecule, Figure 3 shows that the low-lying unoccupied states are at least 2 eV above the Fermi level, at energies much higher than the explored positive bias voltage. For the HS molecule there are several empty states in the range of E_F and E_F +1eV. The density of states is more important for HS molecule, for the LS molecule the empty states close to the Fermi level are mainly centered on the gold surface, but they don't spread enough to the vacuum to be probed by the STM tip. Then in positive bias, only the HS molecules can be imaged by STM. [11] Both LS and HS molecules present occupied states close to the Fermi level, although the density of states is more important for LS molecule (Figure 3). Then in negative bias, where the electrons flow from the occupied states of the sample to the tip, both molecules can be imaged by STM, as observed experimentally.[11] Figure 5 shows the simulated STM images at constant height from the surface (12 Å) with an applied positive (V= +1V) or negative (V= -1V) bias voltage. The STM

12

images are simulated on the basis of the DOS provided by our rPBE calculations, and correctly reproduce all the experimental observation. For positive bias, the STM image for LS molecules is completely dark, and only the HS molecules bright. For negative bias, the spots are brighter for the LS molecules than for the HS ones, in line with the higher density of states of the LS state. Also the shape of the spots indicates a larger contribution of the ligand states for the LS than for the HS molecules. The spots also reflect the C_{3v} symmetry of the scorpionate ligand. These features are also in line with the differences found for the tunneling conductance of LS and HS molecules (see below).
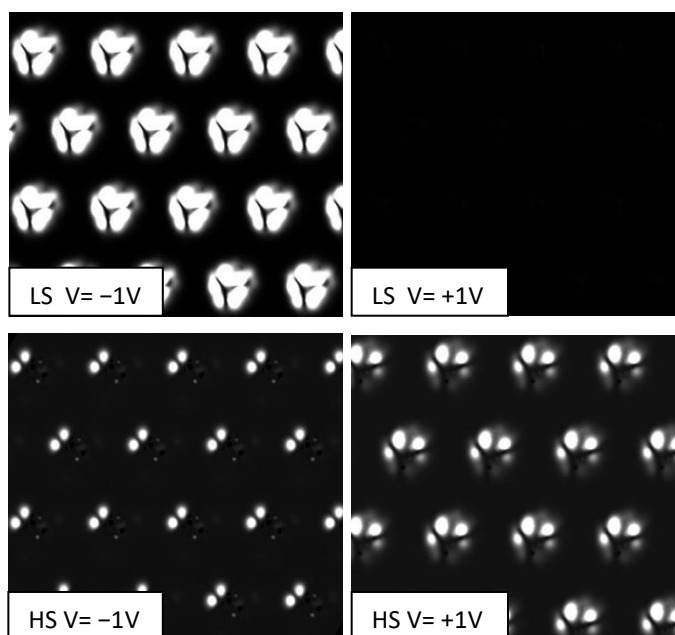

Figure 5. Constant height simulated STM images for LS state and HS states at negative (left) and positive (right) bias voltage of $\pm 1V$.

Transport properties

We have first analyzed the transport properties of each junction at zero bias voltage. The spin and energy-resolved transmission spectra and Green function projected density of states (GF-PDOS) are shown in Figure 6. The calculations were carried out using the PBE functional and this introduces slight differences on the projected DOS around the Fermi level with respect to those shown in Figure 3, but the discrepancies are not relevant for the main features of the transport properties.

In the case of the system with the HS complex as molecular bridge, a spin down transmission peak is observed near the Fermi level (Figure 6a). Inspecting the density of state of the junction projected on the molecule, a sharp peak in the Fe states can also be appreciated (Figure 6b), centered at the same energy value than the transmission resonance. Hence, the transport at negative bias is carried out through the molecule spin-down HOMO, with a strong Fe nature, mainly Fe $3dz^2$ (Figure 4).

13

For the junction featuring the LS complex, two spin-degenerated transmission peaks are observed in the proximity of the Fermi level (Figure 6c), at lower energy than in the HS case, but much more higher in intensity (about one order higher), in line with the higher density of states centered on the LS molecule below the Fermi level. As in the HS molecule, the PDOS on the complex exhibits sharp peaks at the resonant transmission energies (Figure 6d). However, this time, a significant contribution from the nitrogen and carbon atoms of the complex is observed. Thus, it is expected that in this case the almost degenerate HOMO and HOMO-1 orbitals of the complex play a chief role in the junction transport characteristics. These MOs are mainly of Fe d-type character, but with a contribution of the ligands (Figure 4). This delocalization toward the ligands of the resonant orbitals explains the increase of the LS transmission coefficients, due to the improvement of the hybridization between the molecule and the electrodes.
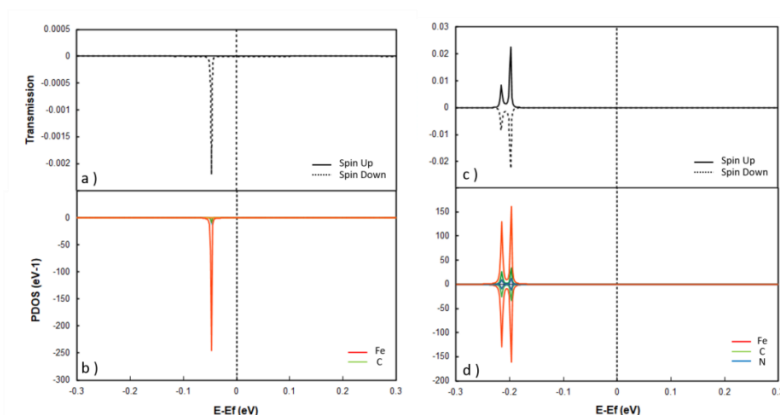

Figure 6. Simulated transmission spectra (a,c) and projected density of states (b,d) for the HS (left) and LS (right) molecules.

Finally, the current through each junction was computed at different negative bias voltages (Figure 7). The calculated I-V profile qualitatively reproduced the results obtained by Bairagi *et al*.[11], showing a higher current for the HS system at low voltages values, and a dramatic increase of the current in the LS configuration after certain voltage threshold. It is worth to mention that, in the low voltage regime, the current through the HS spin junction is completely spin-polarized. This behavior is mainly due to the fact that when a potential difference V is enforced between the electrodes, only the states in a range from -V/2 to V/2 eV, with respect to the Fermi level, are involved in the actual electron transfer. Specifically, this is reflected when the transmission peaks enter in this bias voltage window. In this case, the HS system exhibits larger current values when a small voltage difference is applied, due to the presence of the spin-down transmission peak at around -0.05 eV, along with the almost total absence of transmission signals for the LS system until applying approximately -0.3 V, where two strong and spin-degenerate signals enter the bias window, dramatically increasing the measured current in the low spin configuration.

For the explored bias voltage (-0.3V to 0V) the simulated tunneling current is almost three times smaller than the experimental one. Together to the intrinsic limitations of our I-V simulations, the discrepancies can be also related to differences in the relative position of the tip with respect to the molecule. In our simulation we have fixed the tip along the B-Fe-B axis

14

as in the experiments, separated by 10 Å to the Fe atom, about 4.6 Å from the closest H atom. The available experimental data did not indicate the separation between the tip and the molecule. Since the tunneling current shows an exponential decay with the tip-sample distance, if the distance in our simulation is overestimated by 1 Å, the current would be lessened by a factor of 2.7, close to the ratio between the experimental and simulated current values in the range of bias voltages inspected by our calculations.
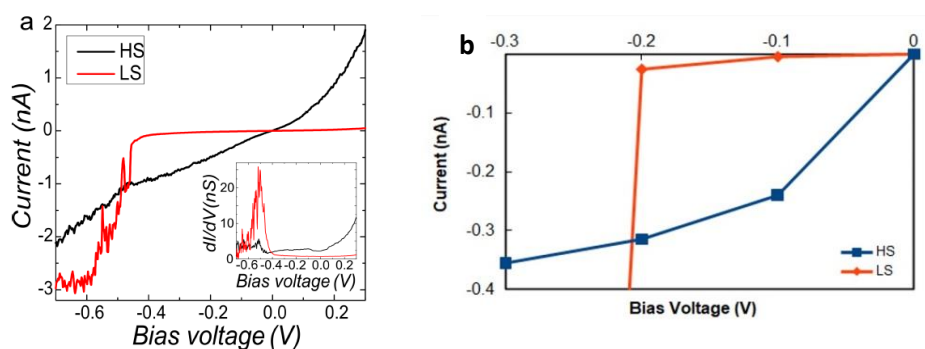

Figure 7. Experimental (a) and simulated (b) I-V curves at constant height for the HS (black) and LS (red) molecule. Experimental I-V reproduced from Ref. [11] (Bairagi *et al*. Nat. Commun. **2016**, *7*, 12212)

LIESST and UV-spectra

The UV-vis absorption spectra registered on the Fe-pz molecular crystal at room temperature[20a, 75] match with the spectra of thick-films,[18] with a strong UV band at about ~220-280 nm (219 nm in the case of thick-films). Upon cooling, at 103 K two well-resolved bands at 349 nm and 278 nm appear, assigned to LS absorptions.[18] The calculated UV-vis spectra for the isolated molecule in the LS (red curve) and HS (green curve) states are shown in Figure 8. The distinctive LS band appears at 475 nm, redshifted by about 100 nm with respect to the experimental spectra at low temperature. This band could be assigned to the transition between the HOMO and HOMO-1 bands to the LUMO of the LS molecule, separated by about 2.2-2.8 eV as shown in Figure 3. The LUMO of the LS molecule presents a notable mixing of Fe 3d and ligand centered bands. In fact, this transition has been assigned to a metal-to-ligand charge transfer absorption band in literature.[20]
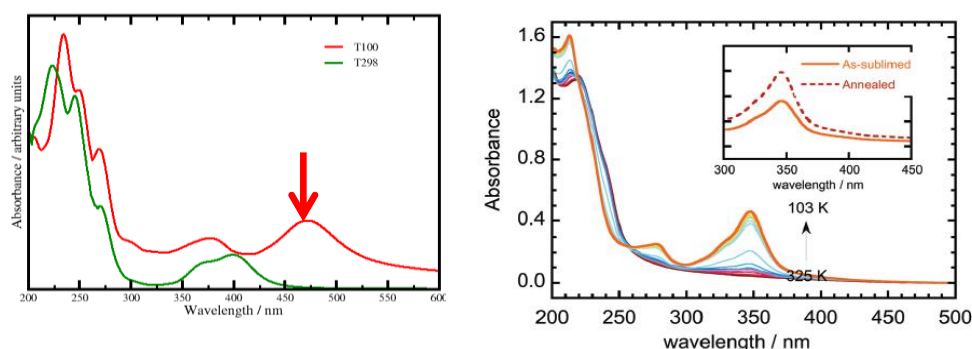

Figure 8. (left) Simulated UV-vis spectra of the LS (red) and HS (green) molecules. (right) Absorption spectra recorded upon cooling of the as-sublimed 130 nm-thick layer of Fe-pz. Reproduced from Ref. [18] with permission from the Royal Society Chemistry.

15

The Fe-pz complex deposited on Au(111) exhibits a light-induced excited spin state trapping (LIESST) phenomenon when illuminated with a blue laser (405 nm) at 4.4 K[17, 21] The laser irradiation induces the conversion from LS to HS, up to a value of 69% of molecules in HS state. The photoexcited state is also a mixed spin-state phase with only one-half of the molecule in HS[11]. The energy of the blue laser corresponds to the low-energy side of the LS distinctive band centered at about 350 nm in the UV-vis spectra at low temperature, and due to the transition from HOMO to LUMO, as indicated the DOS of the LS molecule deposited on Au(111) (Figure 3). The reverse transition HS→ LS takes place for wavelengths about 600 nm.[17]

The light induced LS→ HS transition arises from an individual molecule-photon interactions without role of cooperative effects[7]. This result is in agreement with LIESST in bulk SCMs, where it is also found to be a single-molecule phenomenon.[76] Then it is pertinent to analyze the process on the basis of a single molecule. To explore the photoinduced spin transition in Fe-pz, the low-lying excited states have been calculated as a function of the average Fe-N distance. Figure 9 collects the energy of the five lowest singlet (blue curves), triplet (green curves) and quintet states (red curves) at NEVTP2 level. The model employed to analyze the reaction path correctly simulates the curvature of the singlet and quintet ground states, higher for the singlet than for the quintet, as expected, although the quintet equilibrium distance in our model appears displaced to shorter Fe-N distances than the experimental X-ray high-temperature data, probably due to the imposed constrains. The model, however, exactly matches the experimental low-temperature structure. The spring constants resulting from parabolic fits for the ground singlet and quintet states are k_{LS}=180 eV/Å^2 and k_{HS}=164 eV/ Å^2, twice larger than those previously obtained from DFT+U calculations.[24]

At the equilibrium geometry of the ground singlet, only the vertical transition to the highest singlet S_4 can drive the conversion to the HS state, through an intersystem crossing[76] with the quasi-degenerate quintets Q_3 and Q_4. The intermediate triplets do not seem to be involved in the deactivation of the excited singlet, as occurs in an ideal octahedral geometry.[39] Figure 9 shows a tentative channel for the LS→ HS transition. The vertical excitation S_0→ S_4 at this level of calculation corresponds to 376 nm, close to the blue laser wavelength. The wavefunction of the S_4 state is dominated by single excitations from the Fe 3d t_{2g}-like orbitals to the unoccupied e_g-like ones. Although formally d-d, the non-negligible contribution of the ligand to the nominally Fe e_g-like orbitals could explain the assignment in literature as a metal-to-ligand charge transfer excitation.[20a, 75] The crossing with the excited quintet state takes place at an average Fe-N distance of 2.03Å, although the positions of the crossings between the different states are probably not accurate enough, as mentioned before. This crossing is followed by the internal conversion and finally the relaxation to the lowest quintet state Q_0. The vertical separation between these quintet states at the equilibrium geometry of Q_4 corresponds to 596 nm, nicely close to the wavelength required for the reverse HS→LS transition (~600 nm).
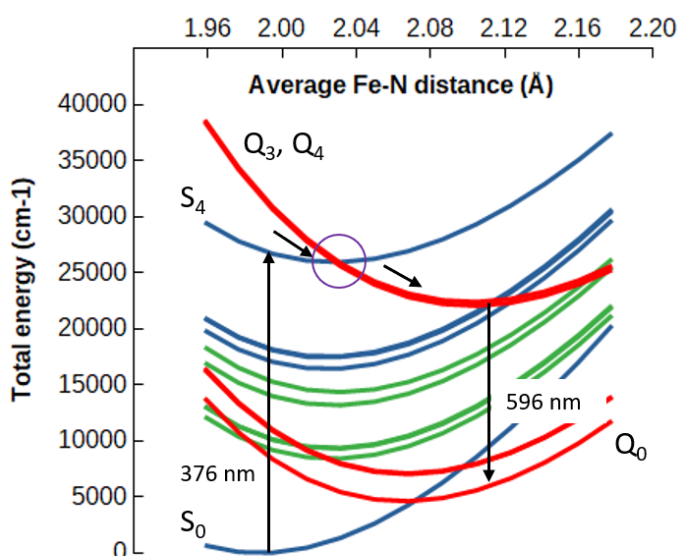
16

Figure 9. Potential energy curves of the low-energy states of the Fe-pz complex as function of the average Fe-N distances. Blue, green and red curves correspond to the singlet, triplet and quintet spin states, respectively.

CONCLUSIONS

The deposition of the Fe-pz complex on Au(111) surface is explored at molecular level through rPBE periodic calculations. The strategy was calibrated against state-of-the-art approaches based on multireference perturbation theories by the evaluation of the LS to HS transition energy. Regarding the computational strategy, the main conclusion of this work is the possibility of eluding the use of the +U approach to study the deposition of SCO Fe complexes on metallic substrates. Our results show that the rPBE functional correctly reproduces not only the HS-LS energy difference, but also captures the main features and singularities of the electronic structure of each spin state. Together with this alternative computational strategy, this study addresses for the first time some aspects of the molecule-substrate interaction such as the differential adsorption energy of the HS and LS molecule, and the key role of the Fe ligand field of each spin state on the behavior of the deposited Fe-pz molecule. This work goes beyond previous studies on the same subject, introducing additional and, in our opinion, general arguments to explain the interaction between the SCO molecules and the substrate.

Our results show that the deposition on the metallic surface is spin-dependent, and favors the LS state. The transition energy is modified by the surface, enhancing the stability of the LS phase. The adsorption energies are in the range of a weak molecule-substrate interaction, at least an order of magnitude smaller than the values reported for the interaction of $Fe(phen)_2(NCS)_2$ with coinage metals,[30] where the molecule is chemically bounded to the surface through the terminal sulfur atoms. A correlation then exists between the strength of the molecule-substrate and the preservation of the SCO properties.

17

This study excludes the thermochemistry of the interaction of each individual molecule with the gold surface as the origin of the observed reduction of the transition temperature and the presence of the mixed HS and LS phase at low temperature. These effects should be related to the activation barriers of the HS→ LS transition, probably modified by the structural constrains imposed by the surface to the molecular layer, as suggest the grazing incidence X-ray diffraction data.[24] The intermolecular interactions in the superstructure formed by the Fe-pz molecules on the surface should also contribute to the stability of this mixed spin phase. Works on both aspects are currently in progress.

The differences in the ligand field of the Fe center on LS and HS states are closely linked to the conductance of each state, since the ligand field affects the position and composition of the states around the Fermi level. The simulated I-V curve agrees with the experimental one, predicting a higher conductance for the HS state for negative bias, until a certain threshold value where the LS current increases dramatically. Also the STM images reflect the differences in the Fe ligand field. The simulated STM images based on the rPBE calculations of a molecule on the surface correctly reproduce the main features of the experimental one. This can be considered as an additional proof of the reliability of these calculations.

Finally, the states involved in the LIESST phenomenon has been identify through NEVPT2 calculations on a model reaction path. The blue light absorption promotes a transition to an excited singlet state that can lead to the HS state through an intersystem crossing with the excited quintet state. A tentative pathway for the photoinduced LS→ HS transition is proposed, that does not involve the intermediate triplet states, and nicely reproduces both the blue laser wavelength for the activation, and the wavelength of the reverse HS→ LS transition.

REFERENCES

[1]   A. Bousseksou, G. Molnár, L. Salmon, W. Nicolazzi, *Chem. Soc. Rev.* **2011**, *40*, 3313-3335.

[2]   A. Cannizzo, C. J. Milne, C. Consani, W. Gawelda, C. Bressler, F. van Mourik, M. Chergui, *Coord. Chem. Rev.* **2010**, *254*, 2677-2686.

18

[3]   K. Senthil Kumar, M. Ruben, *Coord. Chem. Rev.* **2017**, *346*, 176-205.

[4]   J. A. Real, A. B. Gaspar, M. C. Muñoz, *Dalton Trans.* **2005**, 2062-2079.

[5]   H. Naggert, A. Bannwarth, S. Chemnitz, T. von Hofe, E. Quandt, F. Tuczek, *Dalton Trans.* **2011**, *40*, 6364-6366.

[6]   M. Bernien, H. Naggert, L. M. Arruda, L. Kipgen, F. Nickel, J. Miguel, C. F. Hermanns, A. Krüger, D. Krüger, E. Schierle, E. Weschke, F. Tuczek, W. Kuch, *ACS Nano* **2015**, *9*, 8960-8966.

[7]   L. Kipgen, M. Bernien, S. Ossinger, F. Nickel, A. J. Britton, L. M. Arruda, H. Naggert, C. Luo, C. Lotze, H. Ryll, F. Radu, E. Schierle, E. Weschke, F. Tuczek, W. Kuch, *Nat. Commun.* **2018**, *9*, 2984.

[8]   S. Shi, G. Schmerber, J. Arabski, J.-B. Beaufrand, D. J. Kim, S. Boukari, M. Bowen, N. T. Kemp, N. Viart, G. Rogez, E. Beaurepaire, H. Aubriet, J. Petersen, C. Becker, D. Ruch, *Appl. Phys. Lett.* **2009**, *95*, 043303.

[9]   T. Miyamachi, M. Gruber, V. Davesne, M. Bowen, S. Boukari, L. Joly, F. Scheurer, G. Rogez, T. K. Yamada, P. Ohresser, E. Beaurepaire, W. Wulfhekel, *Nat. Commun.* **2012**, *3*, 938.

[10]   M. Gruber, V. Davesne, M. Bowen, S. Boukari, E. Beaurepaire, W. Wulfhekel, T. Miyamachi, *Phys. Rev.B* **2014**, *89*, 195415.

[11]   K. Bairagi, O. Iasco, A. Bellec, A. Kartsev, D. Li, J. Lagoute, C. Chacon, Y. Girard, S. Rousset, F. Miserque, Y. J. Dappe, A. Smogunov, C. Barreteau, M.-L. Boillot, T. Mallah, V. Repain, *Nat. Commun.* **2016**, *7*, 12212.

[12]   H. Naggert, J. Rudnik, L. Kipgen, M. Bernien, F. Nickel, L. M. Arruda, W. Kuch, C. Näther, F. Tuczek, *J. Mater. Chem. C* **2015**, *3*, 7870-7877.

[13]   S. Ossinger, H. Naggert, L. Kipgen, T. Jasper-Toennies, A. Rai, J. Rudnik, F. Nickel, L. M. Arruda, M. Bernien, W. Kuch, R. Berndt, F. Tuczek, *J. Phys. Chem. C* **2017**, *121*, 1210-1219.

[14]   A. Pronschinske, Y. Chen, G. F. Lewis, D. A. Shultz, A. Calzolari, M. Buongiorno Nardelli, D. B. Dougherty, *Nano Lett.* **2013**, *13*, 1429-1434.

[15]   M. Ruben, K. S. Kumar, *Angew. Chem. Int. Ed.* **2020**, *10.1002/anie.201911256*.

[16]   T. Palamarciuc, J. C. Oberg, F. El Hallak, C. F. Hirjibehedin, M. Serri, S. Heutz, J.-F. Létard, P. Rosa, *J. Mater. Chem.* **2012**, *22*, 9690-9695.

[17]   V. Davesne, M. Gruber, M. Studniarek, W. H. Doh, S. Zafeiratos, L. Joly, F. Sirotti, M. G. Silly, A. B. Gaspar, J. A. Real, G. Schmerber, M. Bowen, W. Weber, S. Boukari, V. D. Costa, J. Arabski, W. Wulfhekel, E. Beaurepaire, *J. Chem. Phys.* **2015**, *142*, 194702.

[18]   O. Iasco, M. L. Boillot, A. Bellec, R. Guillot, E. Rivière, S. Mazerat, S. Nowak, D. Morineau, A. Brosseau, F. Miserque, V. Repain, T. Mallah, *J. Mater. Chem. C* **2017**, *5*, 11067-11075.

[19]   V. Shalabaeva, S. Rat, M. D. Manrique-Juarez, A.-C. Bas, L. Vendier, L. Salmon, G. Molnár, A. Bousseksou, *J. Mater. Chem. C* **2017**, *5*, 4419-4425.

[20]   aJ. P. Jesson, S. Trofimenko, D. R. Eaton, *J. Am. Chem. Soc.* **1967**, *89*, 3148-3158; bJ. P. Jesson, S. Trofimenko, D. R. Eaton, *J. Am. Chem. Soc.* **1967**, *89*, 3158-3164.

[21]   K. Bairagi, A. Bellec, C. Fourmental, O. Iasco, J. Lagoute, C. Chacon, Y. Girard, S. Rousset, F. Choueikani, E. Otero, P. Ohresser, P. Sainctavit, M.-L. Boillot, T. Mallah, V. Repain, *J. Phys. Chem. C* **2018**, *122*, 727-731.

[22]   K. Bairagi, A. Bellec, C. Fourmental, Y. Tong, O. Iasco, J. Lagoute, C. Chacon, Y. Girard, S. Rousset, F. Choueikani, E. Otero, P. Ohresser, P. Sainctavit, M.-L. Boillot, T. Mallah, V. Repain, *J. Phys. Chem. C* **2018**, *122*, 29080-29080.

[23]   C. Fourmental, S. Mondal, R. Banerjee, A. Bellec, Y. Garreau, A. Coati, C. Chacon, Y. Girard, J. Lagoute, S. Rousset, M. L. Boillot, T. Mallah, C. Enachescu, C. Barreteau, Y. J. Dappe, A. Smogunov, S. Narasimhan, V. Repain, *J. Phys. Chem. Lett.* **2019**, *10*, 4103-4109.

[24] C. Fourmental, S. Mondal, R. Banerjee, A. Bellec, Y. Garreau, A. Coati, C. Chacon, Y. Girard, J. Lagoute, S. Rousset, M.-L. Boillot, T. Mallah, C. Enachescu, C. Barreteau, Y. J. Dappe, A. Smogunov, S. Narasimhan, V. Repain, *J. Phys. Chem. Lett.* **2019**, *10*, 4103-4109.

[25] S. Lebègue, S. Pillet, J. G. Ángyán, *Phys. Rev.B* **2008**, *78*, 024433.

[26] H. Paulsen, *Magnetochemistry* **2016**, *2*.

[27] S. Vela, M. Fumanal, J. Ribas-Arino, V. Robert, *Phys Chem Chem Phys* **2015**, *17*, 16306-16314.

[28] T. Bučko, J. Hafner, S. Lebègue, J. G. Ángyán, *Phys Chem Chem Phys* **2012**, *14*, 5389-5396.

[29] Y. Zhang, *J. Chem. Phys.* **2014**, *141*, 214703.

[30] S. Gueddida, M. Alouani, *Phys. Rev.B* **2013**, *87*, 144413.

[31] O. S. Siig, K. P. Kepp, *J. Phys. Chem. A* **2018**, *122*, 4208-4217.

[32] K. P. Kepp, *Inorganic Chemistry* **2016**, *55*, 2717-2727.

[33] K. Andersson, P. A. Malmqvist, B. O. Roos, , *J. Chem. Phys.* **1992**, *96*, 1218-1226.

[34] C. Angeli, R. Cimiraglia, S. Evangelisti, T. Leininger, J.-P. Malrieu, *J. Chem. Phys.* **2001**, *114*, 10252-10264.

[35] K. Pierloot, S. Vancoillie, *J. Chem. Phys.* **2008**, *128*, 034104.

[36] B. Ordejón, C. de Graaf, C. Sousa, *J. Am. Chem. Soc.* **2008**, *130*, 13961-13968.

[37] M. Kepenekian, V. Robert, B. Le Guennic, C. De Graaf, *J. Comput. Chem.* **2009**, *30*, 2327-2333.

[38] C. Sousa, C. de Graaf, A. Rudavskyi, R. Broer, *J. Phys. Chem. A* **2017**, *121*, 9720-9727.

[39] N. Suaud, M.-L. Bonnet, C. Boilleau, P. Labèguerie, N. Guihéry, *J. Am. Chem. Soc.* **2009**, *131*, 715-722.

[40] S. Vela, M. Fumanal, J. Ribas-Ariño, V. Robert, *J. Comput. Chem.* **2016**, *37*, 947-953.

[41] a) G. Ghigo, B. O. Roos, P.-Å. Malmqvist, *Chem. Phys. Lett.* **2004**, *396*, 142-149; b) N. Forsberg, P.-Å. Malmqvist, *Chem. Phys. Lett.* **1997**, *274*, 196-204.

[42] J. P. Zobel, J. J. Nogueira, L. González, *Chem. Sci.* **2017**, *8*, 1482-1499.

[43] aM. D. a. N. M. Kroll, *Ann. Phys* **1974**, *82*, 89-155; bB. A. Hess, *Phys. Rev.A* **1986**, *33*, 3742-3748.

[44] F. Aquilante, J. Autschbach, R. K. Carlson, L. F. Chibotaru, M. G. Delcey, L. De Vico, I. Fdez. Galván, N. Ferré, L. M. Frutos, L. Gagliardi, M. Garavelli, A. Giussani, C. E. Hoyer, G. Li Manni, H. Lischka, D. Ma, P. Å. Malmqvist, T. Müller, A. Nenov, M. Olivucci, T. B. Pedersen, D. Peng, F. Plasser, B. Pritchard, M. Reiher, I. Rivalta, I. Schapiro, J. Segarra-Martí, M. Stenrup, D. G. Truhlar, L. Ungur, A. Valentini, S. Vancoillie, V. Veryazov, V. P. Vysotskiy, O. Weingart, F. Zapata, R. Lindh, *J. Comput. Chem.* **2016**, *37*, 506-541.

[45] a) B. O. Roos, R. Lindh, P. A. Malmqvist, V. Veryazov, P. O. Widmark, *J Phys Chem. A* **2005**, *109*, 6575-6579; b) B. O. Roos, R. Lindh, P. A. Malmqvist, V. Veryazov, P. O. Widmark, *J Phys Chem. A* **2004**, *108*, 2851-2858.

[46] C. Angeli, R. Cimiraglia, J.-P. Malrieu, *J. Chem. Phys.* **2002**, *117*, 9138-9153.

[47] F. Neese, *Wiley Interdisciplinary Reviews: Computational Molecular Science* **2012**, *2*, 73-78.

[48] F. Weigend, *Phys Chem Chem Phys* **2006**, *8*, 1057-1065.

[49] E. v. Lenthe, E. J. Baerends, J. G. Snijders, *J. Chem. Phys.* **1993**, *99*, 4597-4610.

[50] D. G. M. Atanasov, K. Sivalingam, F. Neese, *Struct. and Bond.* **2012**, *143*, 149-220.

[51] B. Hammer, L. B. Hansen, J. K. Norskov, *Phys. Rev.B* **1999**, *59*, 7413-7421.

[52] S. Grimme, J. Antony, S. Ehrlich, H. Krieg, *J. Chem. Phys.* **2010**, *132*.

[53] a) G. H. Kresse, J., *Phys. Rev.B* **1993**, *47*, 4; b) G. Kresse, J. Hafner, *Phys. Rev.B* **1994**, *49*, 14251-14269; cG. Kresse, J. Furthmuller, *Comput. Mater. Sci.* **1996**, *6*, 15-50; dG. Kresse, J. Furthmuller, *Phys. Rev.B* **1996**, *54*, 11169-11186.

[54] a) P. E. Blochl, *Phys. Rev.B* **1994**, *50*, 17953-17979; b) G. Kresse, D. Joubert, *Phys. Rev.B* **1999**, *59*, 1758-1775.

20

[55]   H. J. Monkhorst, J. D. Pack, *Phys. Rev.B* **1976**, *13*, 5188-5192.

[56]   J. P. Perdew, K. Burke, M. Ernzerhof, *Phys. Rev.Lett.* **1997**, *78*, 1396-1396.

[57]   Y. K. Zhang, W. T. Yang, *Phys. Rev.Lett.* **1998**, *80*, 890-890.

[58]   J. W. Sun, A. Ruzsinszky, J. P. Perdew, *Phys. Rev. Lett.* **2015**, *115*.

[59]   S. Grimme, *J. Comput. Chem.* **2006**, *27*, 1787-1799.

[60]   J. Tersoff, D. R. Hamann, *Phys. Rev.B* **1985**, *31*, 805-813.

[61]   M. Gajdos, K. Hummer, G. Kresse, J. Furthmuller, F. Bechstedt, *Phys. Rev.B* **2006**, *73,* 045112.

[62]   J. Taylor, H. Guo, J. Wang, *Phys. Rev.B* **2001**, *63*, 245407.

[63]   N. Papior, N. Lorente, T. Frederiksen, A. García, M. Brandbyge, *Comput. Phys. Commun.* **2017**, *212*, 8-24.

[64]   J. M. Soler, E. Artacho, J. D. Gale, A. García, J. Junquera, P. Ordejón, D. Sánchez-Portal, *J Phys Condens Matt.* **2002**, *14*, 2745-2779.

[65]   N. Troullier, J. L. Martins, *Phys. Rev.B* **1991**, *43*, 1993-2006.

[66]   W. Zhao, D. Zou, C.-L. Yang, Z. Sun, *J. Mater. Chem. C* **2017**, *5*, 8862-8868.

[67]   L. L. Tao, J. Wang, *Nanoscale* **2017**, *9*, 12684-12689.

[68]   A. C. Aragonès, D. Aravena, J. I. Cerdá, Z. Acís-Castillo, H. Li, J. A. Real, F. Sanz, J. Hihath, E. Ruiz, I. Díez-Pérez, *Nano Lett.* **2016**, *16*, 218-226.

[69]   D. Aravena, E. Ruiz, *J. Am. Chem. Soc.* **2012**, *134*, 777-779.

[70]   Y. Gu, Y. Hu, J. Huang, Q. Li, J. Yang, *J. Phys. Chem. C* **2019**, *123*, 16366-16372.

[71]   E. Burzurí, A. García-Fuente, V. García-Suárez, K. Senthil Kumar, M. Ruben, J. Ferrer, H. S. J. van der Zant, *Nanoscale* **2018**, *10*, 7905-7911.

[72]   F. Li, J. Huang, Y. Hu, Q. Li, *RSC Adv.* **2019**, *9*, 12339-12345.

[73]   J. Huang, R. Xie, W. Wang, Q. Li, J. Yang, *Nanoscale* **2016**, *8*, 609-616.

[74]   M. Gruber, T. Miyamachi, V. Davesne, M. Bowen, S. Boukari, W. Wulfhekel, M. Alouani, E. Beaurepaire, *J. Chem. Phys.* **2017**, *146*, 092312.

[75]   L. Salmon, G. Molnár, S. Cobo, P. Oulié, M. Etienne, T. Mahfoud, P. Demont, A. Eguchi, H. Watanabe, K. Tanaka, A. Bousseksou, *New J. Chem.* **2009**, *33*, 1283-1289.

[76]   P. Gütlich, A. Hauser, H. Spiering, *Angew. Chem. Int. Ed.* **1994**, *33*, 2024-2054.

Table of contents
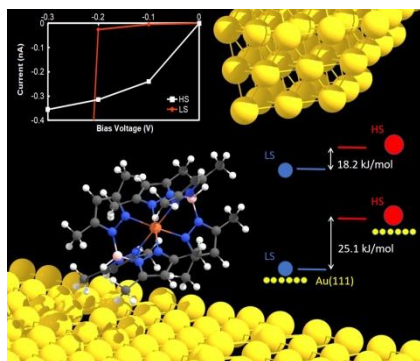
The deposition of $Fe^{II}((3,5-(CH_3)_2Pz)_3BH)_2$ on Au(111) surface is explored through rPBE periodic calculations. The LS→HS transition energy is enhanced by the surface. The adsorption is spin-dependent, and favors the LS state. The different strength of the Fe ligand field at low and high temperature is at the origin of the differential adsorption of the LS and HS molecules, the spin-dependent conductance, and the differences found in the STM images, correctly reproduced from the DOS provided by the rPBE calculations.

Accepted Manuscript

22